

XYScanNet: An Interpretable State Space Model for Perceptual Image Deblurring

Hanzhou Liu¹ Chengkai Liu¹ Jiacong Xu² Peng Jiang¹ Mi Lu¹

Abstract

Deep state-space models (SSMs), like recent Mamba architectures, are emerging as a promising alternative to CNN and Transformer networks. Existing Mamba-based restoration methods process the visual data by leveraging a flatten-and-scan strategy that converts image patches into a 1D sequence before scanning. However, this scanning paradigm ignores local pixel dependencies and introduces spatial misalignment by positioning distant pixels incorrectly adjacent, which reduces local noise-awareness and degrades image sharpness in low-level vision tasks. To overcome these issues, we propose a novel slice-and-scan strategy that alternates scanning along intra- and inter-slices. We further design a new Vision State Space Module (VSSM) for image deblurring, and tackle the inefficiency challenges of the current Mamba-based vision module. Building upon this, we develop XYScanNet, an SSM architecture integrated with a lightweight feature fusion module for enhanced image deblurring. XYScanNet, maintains competitive distortion metrics and significantly improves perceptual performance. Experimental results show that XYScanNet enhances KID by 17% compared to the nearest competitor. Our code will be released soon.

1. Introduction

Single-image deblurring aims to restore a sharp image from a blurred one, typically framed as an inverse filtering problem (Fergus et al., 2006; Pan et al., 2016; Yan et al., 2017; Chen et al., 2019; Zhang et al., 2022). With the rapid development of deep learning, Convolutional Neural Networks (CNNs) (Nah et al., 2017; Kupyn et al., 2018; 2019; Zhang et al., 2019; Suin et al., 2020; Li et al., 2021b;a; Cho et al., 2021; Zamir et al., 2021; Liu et al., 2023) have

¹Texas A&M University, USA ²Johns Hopkins University, USA. Correspondence to: Hanzhou Liu <hanzhou1996@tamu.edu>.

This is the pre-print version of our work to be improved in future.

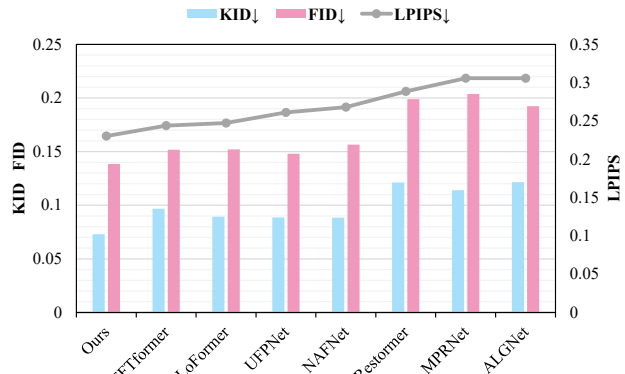


Figure 1. XYScanNet achieves state-of-the-art performance on the GoPro dataset (Nah et al., 2017), measured by the perceptual metrics normalized to [0, 1] for clear visualizations.

become the dominant approach for image deblurring. Recently, Transformer-based models (Zamir et al., 2022; Wang et al., 2022; Tsai et al., 2022; Kong et al., 2023; Mao et al., 2024) have also shown strong performance, leveraging their attention-based mechanisms.

The recent Mamba architectures (Gu & Dao, 2023) combining state-space models (SSMs) with Selective Scan, are emerging as a promising alternative to CNNs and Transformers for vision tasks (Zhu et al., 2024; Liu et al., 2024c). However, existing Mamba-based vision studies use flatten-and-scan strategies to process visual data, resulting in two key challenges, as illustrated in Figure 2 (a). First, short-range dependencies are lost due to the flattening of image patches into a 1D sequence (Guo et al., 2024), known as **local pixel forgetting**. Second, distant pixels are incorrectly placed next to each other, disrupting spatial context, termed as **spatial misalignment**. These issues weaken local noise-awareness and degrade image sharpness, resulting in suboptimal performance on low-level vision tasks.

To address the aforementioned concerns, we use convolutions to mitigate **local pixel forgetting** (Guo et al., 2024), and importantly, propose a novel slice-and-scan strategy that preserves well-aligned spatial relationships, effectively solving **spatial misalignment**. Figure 2 (b) illustrates that our design consists of alternating Intra-Scanners and Inter-

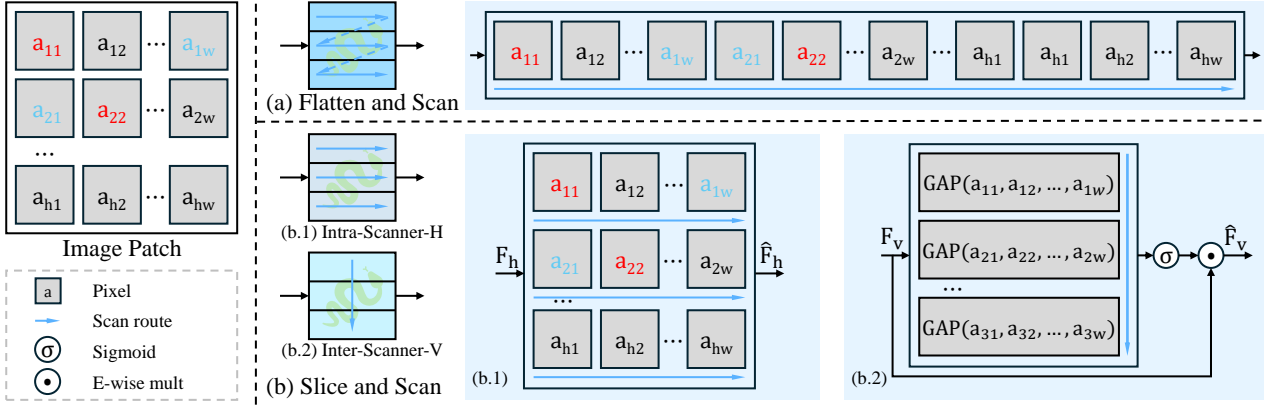


Figure 2. (a) Two issues of flatten-and-scan strategies: adjacent a_{11} and a_{22} become distant (**local pixel forgetting**), while distant a_{1w} and a_{21} are placed adjacent (**spatial misalignment**). (b.1) Intra-Scanner in the horizontal branch; (b.2) Inter-Scanner in the vertical branch, where inter-sliced features are compressed by global average pooling (GAP) for computational efficiency. Intra-Scanner-V and Inter-Scanner-H are symmetrically structured.

Scanners, each made up of horizontal and vertical branches. Intra-Scanners maintain pixel-level clarity (Tsai et al., 2022) while avoiding **spatial misalignment** by preventing direct interactions between misaligned pixels. However, it can be computationally expensive and fails to learn cross-slice dependencies. To overcome these, we introduce Inter-Scanners to efficiently capture relationships among different slices. By integrating these ideas, we propose a novel Vision State Space Module (VSSM) for image deblurring, offering significant improvements in both efficiency and effectiveness over the VSSM in MambaIR (Guo et al., 2024).

Besides, we introduce a lightweight feature fusion module to efficiently leverage multi-level features, using only half the parameters of the AFF (Cho et al., 2021). Combining these advancements, we present XYScanNet, a novel SSM for image deblurring that achieves competitive distortion metrics while markedly enhancing perceptual performance.

The key contributions of this paper are as follows:

- We identify the **spatial misalignment** issue present in prior Mamba-based vision methods and propose a new slice-and-scan approach to address it.
- We develop a novel Vision State Space Module (VSSM) that clearly improves efficiency over the previous Mamba-based vision module.
- We design a deblurring SSM with a lightweight cross-level feature fusion module, achieving competitive distortion metrics and enhanced perceptual performance.

2. Related Work

Single Image Deblurring. Over the past decade, CNN-based methods (Nah et al., 2017; Tao et al., 2018; Zhang

et al., 2019; Li et al., 2021a; Cho et al., 2021; Liu et al., 2023) have become the standard for image deblurring, outperforming traditional approaches (Fergus et al., 2006; Joshi et al., 2009; Zhang et al., 2013; Ren et al., 2016; Pan et al., 2016; Yan et al., 2017; Chen et al., 2019) by leveraging large-scale visual data to learn general priors (Koh et al., 2021; Zhang et al., 2022; Zamir et al., 2021). Inspired by the success of Transformers in Natural Language Processing, recent work has adapted them for low-level computer vision tasks like deblurring (Zamir et al., 2022; Wang et al., 2022; Tsai et al., 2022; Kong et al., 2023; Liu et al., 2024b). For example, the frequency-based network FFTformer (Kong et al., 2023) achieves state-of-the-art PSNR and SSIM scores on mainstream datasets, but demonstrates limited perceptual metrics. In terms of perceptual performance, a diffusion-based approach (Whang et al., 2022) delivers strong metric scores as rated by KID (Kernel Inception Distance) (Bińkowski et al., 2018), FID (Fréchet Inception Distance) (Heusel et al., 2017), LPIPS (Zhang et al., 2019) and NIQE (Mittal et al., 2012), despite its lower distortion metrics. Our state-space model focuses on maintaining competitive distortion metrics and enhancing perceptual scores, distinguishing it from recent deblurring studies that struggle to excel in both aspects.

State Space Models. State-space models (SSMs) have recently seen promising adaptations in deep learning (Gu et al., 2020; 2021b;a; Fu et al., 2022; Smith et al., 2022; Mehta et al., 2022; Gu & Dao, 2023; Poli et al., 2023; Patro & Agneeswaran, 2024). The Linear State-Space Layer (LSSL) (Gu et al., 2021b) introduces improvements in long-term dependency modeling, while the Structured SSM (S4) (Gu et al., 2021a) refines this with a new parameterization to further optimize computational efficiency. However, these early SSMs still face challenges in memorizing information over long sequences. The latest advancement,

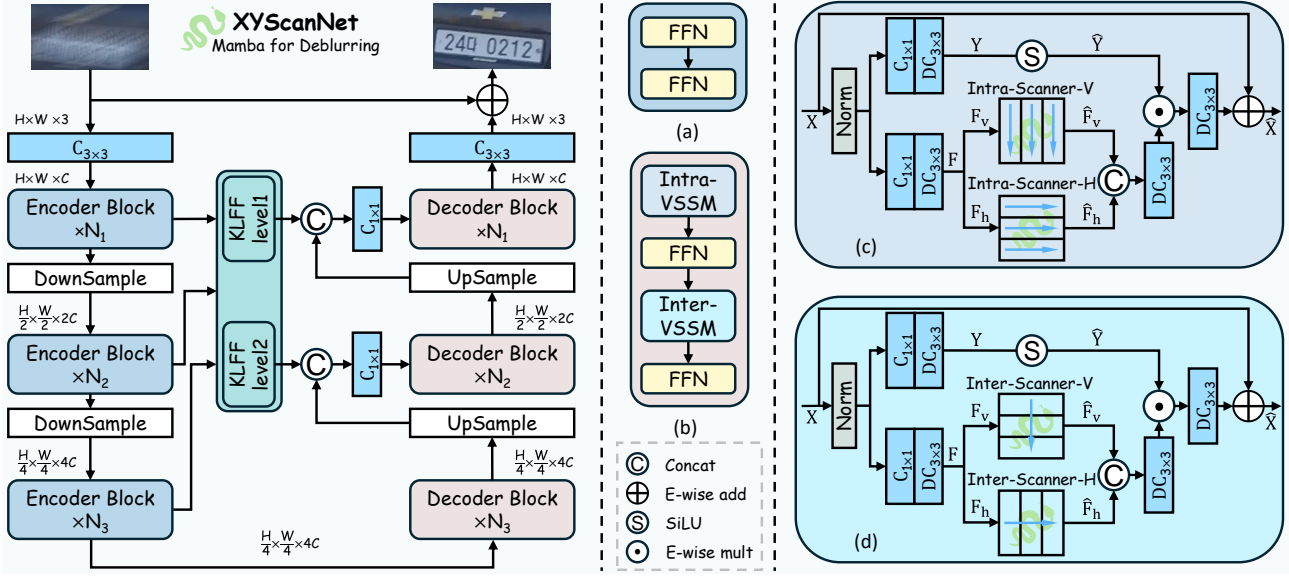


Figure 3. XYScanNet is a three-level U-Net. (a) An encoder block. (b) A decoder block. (c) Intra-VSSM incorporates 3×3 depth-wise convolutions to prevent local pixel forgetting (Guo et al., 2024) and the dual-branch Intra-Scanners (refer to Figure 2 b.1) to address spatial misalignment. (d) Similarly, Inter-VSSM incorporates convolutions and the parallel Inter-Scanners (see Figure 2 b.2).

SSM with Selective Scan (Mamba-S6) (Gu & Dao, 2023), addresses these limitations by enabling selective focus on inputs and optimizing for hardware-aware parallelism, positioning it as a potential alternative to Transformers.

Vision Mamba (Zhu et al., 2024), utilizing bidirectional Mamba blocks, has shown a Transformer-style understanding of high-resolution images while with reduced computational demands. VMamba (Liu et al., 2024c) introduces a 2D Selective Scan (SS2D) module with four-way scanning to enhance visual context capture and achieves linear growth in FLOPs. The pioneering Mamba work for low-level vision, MambaIR (Guo et al., 2024) follows the design of SS2D, and further tackles the **local pixel forgetting** issue by integrating convolutional layers. However, it incurs high computational costs when applied to image deblurring. To improve efficiency, ALGNet (Gao et al., 2024) uses a simplified Mamba branch for global feature capture and a parallel convolutional branch to understand local blurred patterns. However, these previous Mamba studies for vision struggle with **spatial misalignment** due to their flatten-and-scan strategies. In this work, we provide comprehensive comparisons between our proposed Vision State Space Module (VSSM) and its counterpart in MambaIR.

3. Methodology

3.1. Preliminaries

Formulation of State Space Models (SSMs) is presented in Equation (1), involving three time-invariant parameters

(\mathbf{A} , \mathbf{B} , \mathbf{C}) that map a 1-D input $x(t)$ to an output $y(t)$ via an implicit hidden state $h(t)$.

$$\begin{aligned} h'(t) &= \mathbf{A}h(t) + \mathbf{B}x(t) \\ y(t) &= \mathbf{C}h(t). \end{aligned} \quad (1)$$

Structured State Space Models (S4) (Gu et al., 2021a) introduce an additional time-step parameter Δ and a discretization rule (f_A, f_B) so that the models can be computed in a linear recurrence way. Assume that the initial state $h_0 = \overline{\mathbf{B}}x_0$. From Equation (2), the output feature maps y at the timestamp t can be written in convolutional mode.

$$\begin{aligned} y_t &= \sum_{s=0}^t \overline{\mathbf{C}}\overline{\mathbf{A}}^s \overline{\mathbf{B}}x_{t-s} = x_t * (\overline{\mathbf{C}}\overline{\mathbf{A}}^t \overline{\mathbf{B}}) \\ y &= x * \overline{\mathbf{K}} \quad \overline{\mathbf{K}} = (\mathbf{C}\overline{\mathbf{B}}, \mathbf{C}\overline{\mathbf{A}}\overline{\mathbf{B}}, \dots, \mathbf{C}\overline{\mathbf{A}}^{T-1}\overline{\mathbf{B}}), \end{aligned} \quad (2)$$

where $\overline{\mathbf{K}}$ denotes the SSM convolution kernel.

Selective State Space Models (Mamba-S6) (Gu & Dao, 2023) introduce time-varying parameters ($\Delta_t, \mathbf{A}_t, \mathbf{B}_t, \mathbf{C}_t$) to replace the constant counterparts in S4 (Gu et al., 2021a). The time-dependent parameters alter the SSM equations, meaning the output y can no longer be expressed in the form of a convolution formula as Equation (2). To this end, a hardware-aware Selective Scan technique is proposed and time-varying SSMs are integrated into deep models.

MambaIR (Guo et al., 2024), the pioneering Mamba-based work for low-level vision leverages the advantage of Mamba, ultra-long sequence memorization, to activate more pixels

for image restoration. However, ALGNet (Gao et al., 2024) reports the limited performance of MambaIR on image deblurring tasks, and our experiments further reveal that its core component, Vision State Space Module (VSSM), is inefficient in both training and inference phases.

3.2. Slice and Scan

In this section, we present the core components of XYScanNet, the Intra-Scanner and Inter-Scanner which are based on the slice-and-scan scheme.

Intra-Scanner. As shown in Figure 2 (b.1), from an input tensor $\mathbf{F}_h \in \mathbb{R}^{\hat{B} \times \hat{H} \times \hat{W} \times \frac{\hat{C}}{2}}$, Intra-Scanner-H first slices feature maps along the height dimension and combines it with the batch dimension, yielding a 1D sequence $\mathbf{F}'_h \in \mathbb{R}^{(\hat{B}\hat{H}) \times \hat{W} \times \frac{\hat{C}}{2}}$. This intra-slicing mechanism preserves the original contextual information at each height, mitigating concerns about **spatial misalignment** caused by existing flattening strategies (Gu et al., 2024). Next, we employ the Mamba-S6 algorithm with Selective Scan (Gu & Dao, 2023), outputting feature maps \mathbf{F}'_h . By scanning \mathbf{F}'_h in a unidirectional manner, the Intra-Scanner-H captures pixel-level dependencies and detects motion blur along the horizontal direction. The Intra-Scanner-V, constructed symmetrically, estimates the vertical projection of motion blur. Overall, the outputs of Intra-Scanner-H and -V are computed by:

$$\begin{aligned}\hat{\mathbf{F}}_h &= \text{S6}[\text{Reshape}(\hat{\mathbf{F}}_h, (\hat{B} \times \hat{H}, \hat{W}, \frac{\hat{C}}{2}))] \\ \hat{\mathbf{F}}_v &= \text{S6}[\text{Reshape}(\hat{\mathbf{F}}_v, (\hat{B} \times \hat{W}, \hat{H}, \frac{\hat{C}}{2}))],\end{aligned}\quad (3)$$

where S6 denotes the Mamba-S6 algorithm (Gu & Dao, 2023), and Reshape is a tensor shape transformation.

Inter-Scanner. Solely using Intra-Scanners causes high computational costs due to their pixel-level granularity and miss cross-slice information, which is essential for adaptive blur estimation. Unlike previous intra-slicing methods (Tsai et al., 2022), ours introduces a compression factor δ to improve efficiency. We explain Inter-Scanner-V at first. As shown in Figure 2 (b.2), from an input tensor $\mathbf{F}_v \in \mathbb{R}^{\hat{B} \times \hat{H} \times \hat{W} \times \frac{\hat{C}}{2}}$, the Intra-Scanner-V first slices feature maps along the height dimension and compress the width dimension by a factor of δ . For simplicity, we set δ to $\frac{1}{\hat{W}}$, so that the compression process can be easily implemented by a global average pooling (GAP) layer, yielding a 1D sequence $\mathbf{F}'_v \in \mathbb{R}^{\hat{B} \times \hat{H} \times \frac{\hat{C}}{2}}$. After that, the Mamba-S6 algorithm (Gu & Dao, 2023) is applied to \mathbf{F}'_v , and the resulting features pass through a Sigmoid activation function and is multiplied by the input \mathbf{F}_v , generating the output $\hat{\mathbf{F}}_v$. By scanning \mathbf{F}'_v in a unidirectional manner, Inter-Scanner-V efficiently captures cross-slice dependencies along the vertical direction and enhances the ability to estimate blur with larger

magnitudes. The horizontal Intra-Scanner is constructed symmetrically. Overall, the outputs of Inter-Scanner-V and -H are computed by Equation (4).

$$\begin{aligned}\hat{\mathbf{F}}_v &= \text{Sigmoid}\{\text{S6}[\text{GAP}(\mathbf{F}_v, (\hat{B}, \hat{H}, \frac{\hat{C}}{2}))]\} \odot \mathbf{F}_v \\ \hat{\mathbf{F}}_h &= \text{Sigmoid}\{\text{S6}[\text{GAP}(\mathbf{F}_h, (\hat{B}, \hat{W}, \frac{\hat{C}}{2}))]\} \odot \mathbf{F}_h,\end{aligned}\quad (4)$$

where GAP is global average pooling; S6 denotes Mamba-S6 algorithm with Selective Scan (Gu & Dao, 2023).

3.3. Vision State Space Module

We omit the batch dimension \hat{B} . As shown in Figure 3 (c) and (d), from an input $\mathbf{X} \in \mathbb{R}^{\hat{H} \times \hat{W} \times \hat{C}}$, VSSM first applies a layer normalization and produces two projections \mathbf{Y} and \mathbf{F} by cascaded pixel-wise and depth-wise convolutions; where $\hat{H} \times \hat{W}$ represents the spatial dimension and \hat{C} is the channel number. The feature maps \mathbf{Y} pass through a SiLU activation layer (Hendrycks & Gimpel, 2016; Ramachandran et al., 2017; Elfwing et al., 2018), resulting non-linear features $\hat{\mathbf{Y}}$. Meanwhile, the other features \mathbf{F} is equally divided along the channel dimension, yielding \mathbf{F}_v and \mathbf{F}_h . Motivated by the dual-branch design in (Tsai et al., 2022), our Mamba-based VSSM contains two parallel components, Scanner-Vertical (V) and -Horizontal (H), to estimate motion blur at different angles. These two parallel Scanners produce $\hat{\mathbf{F}}_v$ and $\hat{\mathbf{F}}_h$ correspondingly, which are concatenated and then multiplied by $\hat{\mathbf{Y}}$ for controlled feature propagation (Zamir et al., 2022). Finally, an element-wise multiplication and addition are performed to obtain the output. The overall process of our VSSM is defined in Equation (5).

$$\begin{aligned}\hat{\mathbf{X}} &= \text{SiLU}(\mathbf{Y}) \odot \text{DualScanner}(\mathbf{F}) + \mathbf{X} \\ (\mathbf{Y}, \mathbf{F}) &= W_d W_p \mathcal{L}(\mathbf{X}),\end{aligned}\quad (5)$$

where W_d and W_p represent the depth-wise and pixel-wise convolution; DualScanner denotes Intra- or Inter-Scanners with a dual-branch design, as discussed in Section 3.2.

3.4. Cross Level Feature Fusion

Unlike the asymmetric feature fusion (AFF) (Cho et al., 2021), which relies on traditional convolution designs (refer

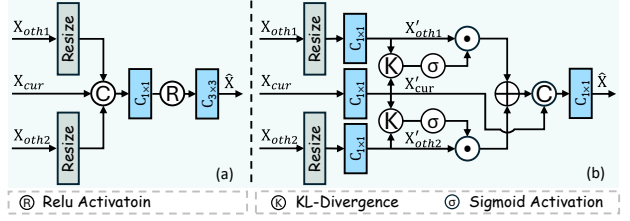


Figure 4. Structures of (a) asymmetric feature fusion (AFF) (Cho et al., 2021), and (b) KL-divergence-based feature fusion (KLFF).

Table 1. Deblurring results on GoPro (Nah et al., 2017). Numbers in red indicate the publication year. XYScanNet evidently outperforms recent deblurring models across all perceptual metrics. For KID and FID, we follow the clean FID implementations (Parmar et al., 2022) and normalize them to a range of [0, 1].

Model	Perceptual ↓				Distortion ↑	
	KID	FID	LPIPS	NIQE	PSNR	SSIM
Ground Truth	0.0	0.0	0.0	3.21	∞	1.000
ACM MM 24						
ALGNet ^{†2}	0.122	0.192	0.089	4.11	33.49	0.964
LoFormer	0.089	0.152	0.072	4.05	34.09	0.969
CVPR 21-24						
MPRNet	0.114	0.204	0.089	4.09	32.66	0.959
DSR-SA ^{*1}	-	-	0.078	<u>4.07</u>	33.23	0.963
Restormer	0.121	0.199	0.084	<u>4.11</u>	32.92	0.961
UFPNet	0.089	<u>0.148</u>	0.076	<u>4.07</u>	34.06	<u>0.968</u>
FFTformer	0.097	0.152	<u>0.071</u>	4.05	34.21	0.969
MISC ^{*1}	-	-	-	-	<u>34.10</u>	0.969
ECCV 22						
NAFNet	<u>0.088</u>	0.157	0.078	<u>4.07</u>	33.71	0.967
Ours						
XYScanNet	0.073	0.138	0.067	4.05	33.91	<u>0.968</u>

to Figure 4 (a)), our proposed KL-divergence-based feature fusion (KLFF) uses only pixel-wise convolutions for efficiency purpose. Besides, we observe that the robustness improvement of AFF over the baseline is limited, likely due to its inability to capture scale discrepancies effectively. To address this, we introduce KL-Divergence to measure the distance between current-level and other-level features, using it as attention scores to better align features and minimize scale discrepancies. The proposed KLFF is illustrated in Figure 4 (b). Given an input feature \mathbf{X}_{cur} from the current level and the other two feature maps \mathbf{X}_{oth1} and \mathbf{X}_{oth2} from different levels, the output $\hat{\mathbf{X}}$ is defined as,

$$\hat{\mathbf{X}} = W_p \{ \{ \text{Sigmoid}[\text{KL}(\mathbf{X}'_{oth1}, \mathbf{X}'_{cur})] \odot \mathbf{X}'_{oth1} + \text{Sigmoid}[\text{KL}(\mathbf{X}'_{oth2}, \mathbf{X}'_{cur})] \odot \mathbf{X}'_{oth2} \} \parallel \mathbf{X}'_{cur} \}, \quad (6)$$

where \mathbf{X}'_{cur} , \mathbf{X}'_{oth1} , \mathbf{X}'_{oth2} denote the projections obtained from resizing and applying pixel-wise convolutions to their respective input features; $\text{KL}(y_{in}, y_{ref})$ represent the KL-Divergence computed by $y_{ref} \cdot (\log y_{ref} - \log y_{in})$; and \parallel denotes feature concatenation.

4. Experiments and Analysis

Evaluation protocols adopted in this paper align with prior deblurring work (Whang et al., 2022; Liu et al., 2024b). These protocols are briefly outlined in the table captions and further clarified in the supplementary materials.

Table 2. Deblurring results of the GoPro-trained networks on HIDE (Shen et al., 2019). While human-centric images elevate NIQE \downarrow (Zvezdakova et al., 2019), XYScanNet clearly strikes a better balance between distortion and the other perceptual metrics.

Model	Perceptual ↓				Distortion ↑	
	KID	FID	LPIPS	NIQE	PSNR	SSIM
Ground Truth	0.0	0.0	0.0	2.72	∞	1.000
MPRNet	0.055	0.168	0.114	3.46	30.96	0.939
DSR-SA ^{*1}	-	-	<u>0.092</u>	2.93	30.07	0.928
NAFNet	0.043	0.137	0.103	3.22	31.31	0.942
Restormer	0.052	0.150	0.108	3.42	31.22	0.942
UFPNet	0.066	0.150	0.093	<u>3.13</u>	<u>31.74</u>	<u>0.947</u>
FFTformer	0.051	0.139	0.096	3.29	31.62	0.945
MISC ^{*1}	-	-	-	-	31.66	0.946
ALGNet ^{†2}	0.083	0.166	0.100	3.20	31.64	<u>0.947</u>
LoFormer	<u>0.040</u>	<u>0.125</u>	0.093	3.30	31.86	0.949
XYScanNet	0.035	0.118	0.091	3.52	<u>31.74</u>	<u>0.947</u>

4.1. Implementation Details

We train XYScanNet on the GoPro (Nah et al., 2017) dataset, evaluating it on GoPro, HIDE (Shen et al., 2019), and RWBI (Zhang et al., 2020) test sets. For this training, we use the Adam (Kingma, 2014) optimizer with an initial learning rate of 2.2×10^{-4} , decaying to 1×10^{-7} following a Cosine Annealing schedule. Data augmentation includes random cropping, flipping, and rotation. Following recent work (Liu et al., 2024a), we set the total number of iterations to 788K. We adopt a simple progressive training strategy (Zamir et al., 2022), starting with a patch size of 252×252 and batch size of 16, which is updated to patch size 320×320 and batch size 8 at iteration 394K. The objective function combines pixel-wise and perceptual loss (Liu et al., 2024b). XYScanNet is trained on 8 NVIDIA A100 GPUs. Training on RealBlur follows the previous setup (Fang et al., 2023).

4.2. Comparisons with State-of-the-art Methods

4.2.1. QUANTITATIVE ANALYSIS

In Table 1-5, the best results are **bolded**, and the second-best results are underlined; ‘-’ represents insufficient information. In case of small discrepancies between our local runs and the reported results, we adhere to the data from the original papers. Refer to Footnotes ¹ ² for more annotations.

GoPro results. We train and evaluate XYScanNet on the GoPro dataset (Nah et al., 2017). The image quality scores of the deblurred results are summarized in Table 1, where XYScanNet consistently outperforms existing deblurring

¹* indicates results taken directly from the paper.

²† denotes results tested on images provided by the authors.

Table 3. Quantitative results of the GoPro-trained networks evaluated on the RWBI testset which contains no reference image.

Method	Blurred	MPRNet	Restormer	NAFNet	UFPNet	FFTformer	LoFormer	XYScanNet
NIQE \downarrow	3.546	3.591	3.594	3.441	3.690	3.384	3.536	3.383

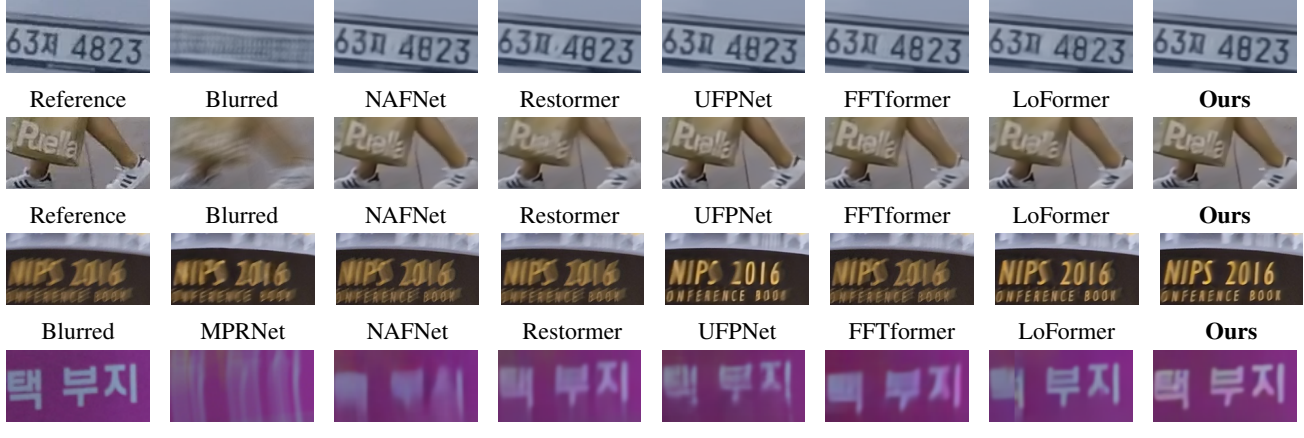


Figure 5. From the top to bottom rows: qualitative comparisons on the GoPro, HIDE, RWBI and RealBlur-J testsets. For the first three row, the deblurring networks are trained only on the GoPro training set and directly applied to GoPro, HIDE and RWBI testsets. For the bottom row, we train and test models on the RealBlur-J dataset. Our XYScanNet produces sharper and visually pleasant results.

Table 4. Perceptual performance of deblurring models trained and tested on RealBlur datasets. Since RealBlur contains misaligned image pairs, to evaluate perceptual performance, we use LPIPS with shift-tolerance and NIQE with no reference image required.

Method	RealBlur-J		RealBlur-R	
	LPIPS st	NIQE	LPIPS st	NIQE
Ground Truth	0.0	3.41	0.0	4.75
MPRNet	0.068	4.11	0.018	5.59
DeepRFT ^{†2}	0.058	3.89	0.016	5.30
UFPNet	0.048	3.94	0.013	5.23
FFTformer	0.047	3.84	0.014	5.45
MISC ^{†2}	0.047	3.80	0.013	5.45
XYScanNet	0.041	3.71	0.012	5.21

networks across all perceptual metrics while maintaining a competitive PSNR of 33.91 dB and SSIM of 0.968. Notably, XYScanNet achieves a KID score of 0.073, nearly a 25% reduction compared to FFTformer (Kong et al., 2023) with the highest distortion metrics on the GoPro testset, demonstrating that our method achieves state-of-the-art deblurring performance in terms of perceptual metrics on GoPro.

HIDE results. We directly apply the GoPro-trained networks to the HIDE testset (Shen et al., 2019), which primarily consists of human images, to assess their generalization capabilities to broader domains. As shown in Ta-

ble 2, XYScanNet achieves the second-highest PSNR of 31.74 dB and SSIM of 0.947, closely following the latest LoFormer (Mao et al., 2024). While it has been reported that the fine facial textures in human centric images elevate NIQE values (Zvezdakova et al., 2019), we report NIQE for thorough comparisons. Table 2 reports that XYScanNet surpasses recent networks across nearly all perceptual metrics except NIQE on HIDE, suggesting the effectiveness of our approach to process blurred images focused on people.

RWBI results. We further assess generalization capabilities of the GoPro-trained models on the RWBI dataset (Zhang et al., 2020) which features real-world blur and contains no ground-truth image, metric scores of which are reported in Table 3. MPRNet (Zamir et al., 2021), Restormer (Zamir et al., 2022), and UFPNet (Fang et al., 2023) generate deblurred images with higher NIQE scores than the original blurred inputs, indicating reduced naturalness. In contrast, networks like NAFNet (Chen et al., 2022), LoFormer (Mao et al., 2024), FFTformer (Kong et al., 2023), and XYScanNet achieve lower NIQE scores, reflecting improved deblurring quality. XYScanNet achieves the highest NIQE reduction of 0.163, surpassing NAFNet’s 0.105, LoFormer’s 0.01, and performing competitively with FFTformer’s 0.162. It indicates the powerful generalization of XYScanNet to the images with real-world blurred patterns.

RealBlur results. To further investigate the perceptual performance of XYScanNet across diverse blurred scenes, we

Table 5. Comparison of the vision module from MambaIR and ours on image deblurring datasets. Our method achieves noticeable perceptual metric improvements, except for KID on the GoPro dataset (Nah et al., 2017) and LPIPS on the HIDE dataset (Shen et al., 2019), with significantly enhanced efficiency. Networks are only trained on the GoPro dataset. T denotes time and S represents space.

Method	GoPro				HIDE				RWBI	#Param. (M)	Training T (s)	Training S (GB)	Inference T (s)	Inference S (GB)
	KID	FID	LPIPS	NIQE	KID	FID	LPIPS	NIQE						
Reference	0.0	0.0	0.0	3.21	0.0	0.0	0.0	2.72	-	-	-	-	-	-
MambaIR	0.121	0.232	0.094	4.06	0.074	0.201	0.121	3.46	3.63	7.41	189	17.39	0.196	8.38
Ours	0.129	0.210	0.091	4.06	0.064	0.188	0.122	3.41	3.51	7.30	82	11.60	0.165	4.51

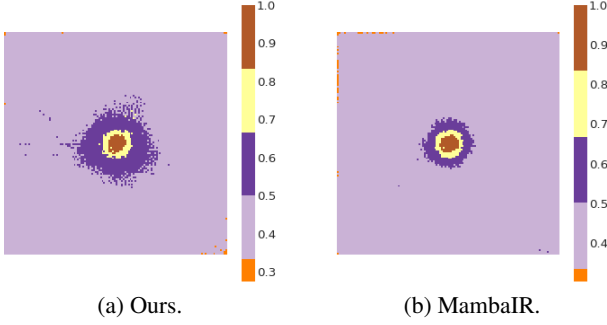


Figure 6. Effective receptive fields (ERFs) of XYScanNet with (a) our VSSMs based on slice-and-scan and (b) the VSSMs adopted in MambaIR (Guo et al., 2024). Ours has a sparser ERF with more intensive pixels compared to the MambaIR method.

Network	GoPro	HIDE	RWBI	RB.-J	RB.-R
UFNet	0.708		0.572	0.245	
FFTformer	0.707		0.461	0.236	
LoFormer	0.707		0.592	0.251	
XYScanNet	0.710		0.601	0.266	

Table 6. We are still verify QAlign evaluation results and will report more in future. Please stay tuned.

additionally train it on the RealBlur datasets (Rim et al., 2020), which consist of misaligned image pairs captured in real-world scenarios and provide a challenging benchmark for evaluating deblurring performance. Following previous work (Liu et al., 2024b), we employ Shift-Tolerant-LPIPS (ST-LPIPS) (Ghildyal & Liu, 2022) to evaluate image quality on the RealBlur datasets. Besides, NIQE without reference images needed is used to assess naturalness of the restored images. Table 4 reports that XYScanNet surpasses recent models in ST-LPIPS, indicating a closer alignment with human perception on RealBlur. Moreover, improved NIQE scores validate the enhanced naturalness of our model’s results across multiple real-world scenes.

LLM-based QAlign Score. A recent image quality assessment (IQA) method, Q-Align (Wu et al., 2023), is a robust visual scorer based on Large Multi-modality Mod-

els (LMMs). We evaluate recent deblurring networks on mainstream datasets with QAlign and report them in Table 6. We are still working on verifying Q-Align metric and **appreciate any suggestion on QAlign**. Table 6 shows that XYScanNet demonstrates the best overall performance.

4.2.2. QUALITATIVE ANALYSIS

Figure 5 highlights the limitations of existing CNN and Transformer methods (Zamir et al., 2021; Chen et al., 2022; Fang et al., 2023; Zamir et al., 2022; Kong et al., 2023; Mao et al., 2024) in processing severely blurred images. These approaches fall short in restoring sharp edges, clear characters, and distinct patterns from such inputs. By contrast, our Mamba-based method effectively recovers these elements, producing images perceptually closer to the ground truth with noticeably enhanced visual quality. Furthermore, improved visual quality on HIDE (Shen et al., 2019) and RWBI (Zhang et al., 2020) datasets demonstrate XYScanNet’s superior generalization capabilities. The bottom row of Figure 5 proves that XYScanNet also shows high deblurring performance in real-world scenarios. More specifically, our proposed XYScanNet exhibits superior deblurring performance at the edges of local regions, particularly on the characters and geometric designs with high contrast against the background. This is attributed to a better understanding of pixel dependencies in blurred images.

4.3. Ablation Study

For the ablation studies, we train the networks on the GoPro dataset (Nah et al., 2017) with image patches of size 128×128 for 3K epochs. Each model is trained four times, and the average quality metrics are computed and reported. We measure efficiency using the GoPro dataset on a local RTX 3090 GPU. Tables 6-9 show that our contributions enhance image quality and improve computational efficiency. Additional discussions about evaluation methods and more visual results are available in supplementary materials.

Analysis on vision state-space modules. As shown in Figure 6, XYScanNet with our proposed Vision State Space Module (VSSM) has a larger receptive field than the previ-



Figure 7. Qualitative comparisons of the proposed vision module versus the previous VSSM in MambaIR (Guo et al., 2024) on GoPro (Nah et al., 2017) and HIDE (Shen et al., 2019) datasets. Our method generates sharper edges.

Table 7. Comparisons among the inter-only, intra-only and hybrid approaches. The hybrid approach achieves the best balance between quality metrics and computational efficiency.

Intra	Inter	PSNR↑		Time (s)		Space (GB)	
		GoPro	HIDE	Train	Test	Train	Test
✓		31.91	30.01	65	0.153	10.36	3.82
✓		32.18	30.13	103	0.167	12.82	4.67
✓	✓	<u>32.11</u>	<u>30.11</u>	<u>82</u>	<u>0.165</u>	<u>11.60</u>	<u>4.51</u>

ous VSSM adopted in MambaIR (Guo et al., 2024). Visual results in Figure 7 demonstrate that the previous flatten-and-scan based VSSM in MambaIR struggles to restore clear details at the the local region’s edges. We attribute this limitation to **spatial misalignment** which causes misunderstandings of pixel positions. In contrast, our VSSM, utilizing a slice-and-scan method, successfully avoids this issue and restores sharper edges. Table 5 shows that the proposed VSSM reaches the best balance between perceptual metrics and computational costs. Specifically, our method reduces the previous Mamba approach’s training time by **56.61%** and inference memory usage by **46.18%**, while maintaining comparable and even improved perceptual scores.

Investigation of intra- and inter-slices. As reported in Table 7, the combined intra- and inter-method improves PSNR on GoPro (Nah et al., 2017) by 0.2 dB over the inter-only method. Although it shows a minor PSNR reduction of 0.07 dB on GoPro (Nah et al., 2017) and 0.02 dB on HIDE (Shen et al., 2019) compared to intra-only approach, it achieves a 20.39% reduction in training time and a 9.52% decrease in memory usage, highlighting its significant efficiency. Supplementary materials show the hybrid approach’s superior handling of real-world blur.

Effect of cross-level feature fusion. Cross-level feature fusion is primarily designed to enhance model robustness and generalization abilities. Table 8 shows that our KLFF no-

Table 8. Effects of cross-level feature fusion methods. FLOPS and Params indicate the number of floating-point operations and model parameters for the AFF (Cho et al., 2021) or KLFF modules.

AFF	Ours	NIQE↓		LPIPS↓		Flops	Params
		HIDE	RWBI	HIDE	RB.J		
		3.46	<u>3.52</u>	0.125	0.889	-	-
✓		3.40	3.53	<u>0.124</u>	<u>0.878</u>	4.32	152.35
	✓	<u>3.41</u>	3.51	0.122	0.848	2.19	71.43

ticeably reduces NIQE by 0.05 on HIDE (Shen et al., 2019) and LPIPSst by 0.041 on RealBlur-J (Rim et al., 2020), demonstrating superior generalization ability compared to conventional skip connections. Additionally, compared to the AFF method (Cho et al., 2021), our approach reduces FLOPS by **49.3%** and Params by **53.11%**, demonstrating the efficiency of KLFF. Refer to supplementary materials for more comparison results.

5. Conclusion

In this work, we present a deblurring State-Space-Model, XYScanNet, which effectively restores clean images closely aligned with human perception. Specifically, aiming to resolve the spatial misalignment issue caused by the flatten-and-scan methods in Mamba for vision, we introduce a novel slice-and-scan mechanism. Building on this new approach and conventional convolutions, we propose a new Vision State Space Module (VSSM) which demonstrates significantly improved efficiency compared to the previous Mamba-based vision module. Besides, a lightweight cross-level feature fusion module is designed as an alternative to the previous method. Experimental results on multiple synthetic and real-world datasets reveal that XYScanNet achieves state-of-the-art perceptual quality and competitive distortion metrics across diverse scenes.

Impact Statement

This paper focuses on improving the perceptual performance of deblurring networks, with experimental results demonstrating that our method achieves state-of-the-art performance. However, the misuse of image deblurring techniques can lead to negative impacts, including the exposure of sensitive data through deblurred surveillance images, the alteration of original patterns critical for camera identification, and the disruption of logos and watermarks vital to commercial copyrights. We call on the deblurring community to address these challenges and advocate for the responsible application of deblurring technologies.

References

Bińkowski, M., Sutherland, D. J., Arbel, M., and Gretton, A. Demystifying mmd gans. *arXiv preprint arXiv:1801.01401*, 2018.

Chen, L., Fang, F., Wang, T., and Zhang, G. Blind image deblurring with local maximum gradient prior. In *Proceedings of the IEEE/CVF conference on computer vision and pattern recognition*, pp. 1742–1750, 2019.

Chen, L., Chu, X., Zhang, X., and Sun, J. Simple baselines for image restoration. In *European conference on computer vision*, pp. 17–33. Springer, 2022.

Cho, S.-J., Ji, S.-W., Hong, J.-P., Jung, S.-W., and Ko, S.-J. Rethinking coarse-to-fine approach in single image deblurring. In *Proceedings of the IEEE/CVF international conference on computer vision*, pp. 4641–4650, 2021.

Elfwing, S., Uchibe, E., and Doya, K. Sigmoid-weighted linear units for neural network function approximation in reinforcement learning. *Neural networks*, 107:3–11, 2018.

Fang, Z., Wu, F., Dong, W., Li, X., Wu, J., and Shi, G. Self-supervised non-uniform kernel estimation with flow-based motion prior for blind image deblurring. In *Proceedings of the IEEE/CVF conference on computer vision and pattern recognition*, pp. 18105–18114, 2023.

Fergus, R., Singh, B., Hertzmann, A., Roweis, S. T., and Freeman, W. T. Removing camera shake from a single photograph. In *ACM transactions on graphics (TOG)*, volume 25, pp. 787–794. ACM, 2006.

Fu, D. Y., Dao, T., Saab, K. K., Thomas, A. W., Rudra, A., and Ré, C. Hungry hungry hippos: Towards language modeling with state space models. *arXiv preprint arXiv:2212.14052*, 2022.

Gao, H., Ma, B., Zhang, Y., Yang, J., Yang, J., and Dang, D. Learning enriched features via selective state spaces model for efficient image deblurring. In *Proceedings of the 32nd ACM International Conference on Multimedia*, pp. 710–718, 2024.

Ghildyal, A. and Liu, F. Shift-tolerant perceptual similarity metric. In *European Conference on Computer Vision*, pp. 91–107. Springer, 2022.

Gu, A. and Dao, T. Mamba: Linear-time sequence modeling with selective state spaces. *arXiv preprint arXiv:2312.00752*, 2023.

Gu, A., Dao, T., Ermon, S., Rudra, A., and Ré, C. Hippo: Recurrent memory with optimal polynomial projections. *Advances in neural information processing systems*, 33: 1474–1487, 2020.

Gu, A., Goel, K., and Ré, C. Efficiently modeling long sequences with structured state spaces. *arXiv preprint arXiv:2111.00396*, 2021a.

Gu, A., Johnson, I., Goel, K., Saab, K., Dao, T., Rudra, A., and Ré, C. Combining recurrent, convolutional, and continuous-time models with linear state space layers. *Advances in neural information processing systems*, 34: 572–585, 2021b.

Guo, H., Li, J., Dai, T., Ouyang, Z., Ren, X., and Xia, S.-T. Mambair: A simple baseline for image restoration with state-space model. *arXiv preprint arXiv:2402.15648*, 2024.

Hendrycks, D. and Gimpel, K. Gaussian error linear units (gelus). *arXiv preprint arXiv:1606.08415*, 2016.

Heusel, M., Ramsauer, H., Unterthiner, T., Nessler, B., and Hochreiter, S. Gans trained by a two time-scale update rule converge to a local nash equilibrium. *Advances in neural information processing systems*, 30, 2017.

Joshi, N., Zitnick, C. L., Szeliski, R., and Kriegman, D. J. Image deblurring and denoising using color priors. In *2009 IEEE Conference on Computer Vision and Pattern Recognition*, pp. 1550–1557. IEEE, 2009.

Kingma, D. P. Adam: A method for stochastic optimization. *arXiv preprint arXiv:1412.6980*, 2014.

Koh, J., Lee, J., and Yoon, S. Single-image deblurring with neural networks: A comparative survey. *Computer Vision and Image Understanding*, 203:103134, 2021.

Kong, L., Dong, J., Ge, J., Li, M., and Pan, J. Efficient frequency domain-based transformers for high-quality image deblurring. In *Proceedings of the IEEE/CVF Conference on Computer Vision and Pattern Recognition*, pp. 5886–5895, 2023.

Kupyn, O., Budzan, V., Mykhailych, M., Mishkin, D., and Matas, J. Deblurgan: Blind motion deblurring using conditional adversarial networks. In *Proceedings of the IEEE conference on computer vision and pattern recognition*, pp. 8183–8192, 2018.

Kupyn, O., Martyniuk, T., Wu, J., and Wang, Z. Deblurgan-v2: Deblurring (orders-of-magnitude) faster and better. In *Proceedings of the IEEE/CVF international conference on computer vision*, pp. 8878–8887, 2019.

Li, B., Hua, Y., and Lu, M. Advanced multiple linear regression based dark channel prior applied on dehazing image and generating synthetic haze. *arXiv preprint arXiv:2103.07065*, 2021a.

Li, J., Tan, W., and Yan, B. Perceptual variousness motion deblurring with light global context refinement. In *Proceedings of the IEEE/CVF international conference on computer vision*, pp. 4116–4125, 2021b.

Liu, C., Wang, X., Xu, X., Tian, R., Li, S., Qian, X., and Yang, M.-H. Motion-adaptive separable collaborative filters for blind motion deblurring. In *Proceedings of the IEEE/CVF Conference on Computer Vision and Pattern Recognition*, pp. 25595–25605, 2024a.

Liu, H., Li, B., Lu, M., and Wu, Y. Real-world image deblurring via unsupervised domain adaptation. In *International Symposium on Visual Computing*, pp. 148–159, 2023.

Liu, H., Li, B., Liu, C., and Lu, M. Deblurdinat: A lightweight and effective transformer for image deblurring. *arXiv preprint arXiv:2403.13163*, 2024b.

Liu, Y., Tian, Y., Zhao, Y., Yu, H., Xie, L., Wang, Y., Ye, Q., and Liu, Y. Vmamba: Visual state space model. *arXiv preprint arXiv:2401.10166*, 2024c.

Mao, X., Wang, J., Xie, X., Li, Q., and Wang, Y. Loformer: Local frequency transformer for image deblurring. In *Proceedings of the 32nd ACM International Conference on Multimedia*, pp. 10382–10391, 2024.

Mehta, H., Gupta, A., Cutkosky, A., and Neyshabur, B. Long range language modeling via gated state spaces. *arXiv preprint arXiv:2206.13947*, 2022.

Mittal, A., Soundararajan, R., and Bovik, A. C. Making a “completely blind” image quality analyzer. *IEEE Signal processing letters*, 20(3):209–212, 2012.

Nah, S., Hyun Kim, T., and Mu Lee, K. Deep multi-scale convolutional neural network for dynamic scene deblurring. In *Proceedings of the IEEE conference on computer vision and pattern recognition*, pp. 3883–3891, 2017.

Pan, J., Sun, D., Pfister, H., and Yang, M.-H. Blind image deblurring using dark channel prior. In *Proceedings of the IEEE conference on computer vision and pattern recognition*, pp. 1628–1636, 2016.

Parmar, G., Zhang, R., and Zhu, J.-Y. On aliased resizing and surprising subtleties in gan evaluation. In *Proceedings of the IEEE/CVF Conference on Computer Vision and Pattern Recognition*, pp. 11410–11420, 2022.

Patro, B. N. and Agneeswaran, V. S. Mamba-360: Survey of state space models as transformer alternative for long sequence modelling: Methods, applications, and challenges. *arXiv preprint arXiv:2404.16112*, 2024.

Poli, M., Massaroli, S., Nguyen, E., Fu, D. Y., Dao, T., Baccus, S., Bengio, Y., Ermon, S., and Ré, C. Hyena hierarchy: Towards larger convolutional language models. In *International Conference on Machine Learning*, pp. 28043–28078. PMLR, 2023.

Ramachandran, P., Zoph, B., and Le, Q. V. Swish: a self-gated activation function. *arXiv: Neural and Evolutionary Computing*, 2017. URL <https://api.semanticscholar.org/CorpusID:196158220>.

Ren, W., Cao, X., Pan, J., Guo, X., Zuo, W., and Yang, M.-H. Image deblurring via enhanced low-rank prior. *IEEE Transactions on Image Processing*, 25(7):3426–3437, 2016.

Rim, J., Lee, H., Won, J., and Cho, S. Real-world blur dataset for learning and benchmarking deblurring algorithms. In *Proceedings of the European Conference on Computer Vision (ECCV)*, 2020.

Shen, Z., Wang, W., Lu, X., Shen, J., Ling, H., Xu, T., and Shao, L. Human-aware motion deblurring. In *Proceedings of the IEEE/CVF international conference on computer vision*, pp. 5572–5581, 2019.

Smith, J. T., Warrington, A., and Linderman, S. W. Simplified state space layers for sequence modeling. *arXiv preprint arXiv:2208.04933*, 2022.

Suin, M., Purohit, K., and Rajagopalan, A. Spatially-attentive patch-hierarchical network for adaptive motion deblurring. In *Proceedings of the IEEE/CVF conference on computer vision and pattern recognition*, pp. 3606–3615, 2020.

Tao, X., Gao, H., Shen, X., Wang, J., and Jia, J. Scale-recurrent network for deep image deblurring. In *Proceedings of the IEEE conference on computer vision and pattern recognition*, pp. 8174–8182, 2018.

Tsai, F.-J., Peng, Y.-T., Lin, Y.-Y., Tsai, C.-C., and Lin, C.-W. Stripformer: Strip transformer for fast image deblurring. In *European conference on computer vision*, pp. 146–162. Springer, 2022.

Wang, Z., Cun, X., Bao, J., Zhou, W., Liu, J., and Li, H. Uformer: A general u-shaped transformer for image restoration. In *Proceedings of the IEEE/CVF conference on computer vision and pattern recognition*, pp. 17683–17693, 2022.

Whang, J., Delbracio, M., Talebi, H., Saharia, C., Dimakis, A. G., and Milanfar, P. Deblurring via stochastic refinement. In *Proceedings of the IEEE/CVF Conference on Computer Vision and Pattern Recognition*, pp. 16293–16303, 2022.

Wu, H., Zhang, Z., Zhang, W., Chen, C., Liao, L., Li, C., Gao, Y., Wang, A., Zhang, E., Sun, W., et al. Q-align: Teaching lmms for visual scoring via discrete text-defined levels. *arXiv preprint arXiv:2312.17090*, 2023.

Yan, Y., Ren, W., Guo, Y., Wang, R., and Cao, X. Image deblurring via extreme channels prior. In *Proceedings of the IEEE conference on computer vision and pattern recognition*, pp. 4003–4011, 2017.

Zamir, S. W., Arora, A., Khan, S., Hayat, M., Khan, F. S., Yang, M.-H., and Shao, L. Multi-stage progressive image restoration. In *Proceedings of the IEEE/CVF conference on computer vision and pattern recognition*, pp. 14821–14831, 2021.

Zamir, S. W., Arora, A., Khan, S., Hayat, M., Khan, F. S., and Yang, M.-H. Restormer: Efficient transformer for high-resolution image restoration. In *Proceedings of the IEEE/CVF conference on computer vision and pattern recognition*, pp. 5728–5739, 2022.

Zhang, H., Wipf, D., and Zhang, Y. Multi-image blind deblurring using a coupled adaptive sparse prior. In *Proceedings of the IEEE Conference on Computer Vision and Pattern Recognition*, pp. 1051–1058, 2013.

Zhang, H., Dai, Y., Li, H., and Koniusz, P. Deep stacked hierarchical multi-patch network for image deblurring. In *Proceedings of the IEEE/CVF international conference on computer vision*, pp. 5978–5986, 2019.

Zhang, K., Luo, W., Zhong, Y., Ma, L., Stenger, B., Liu, W., and Li, H. Deblurring by realistic blurring. In *Proceedings of the IEEE/CVF conference on computer vision and pattern recognition*, pp. 2737–2746, 2020.

Zhang, K., Ren, W., Luo, W., Lai, W.-S., Stenger, B., Yang, M.-H., and Li, H. Deep image deblurring: A survey. *International Journal of Computer Vision*, 130(9):2103–2130, 2022.

Zhu, L., Liao, B., Zhang, Q., Wang, X., Liu, W., and Wang, X. Vision mamba: Efficient visual representation learning with bidirectional state space model. *arXiv preprint arXiv:2401.09417*, 2024.

Zvezdakova, A., Kulikov, D., Kondranin, D., and Vatolin, D. Barriers towards no-reference metrics application to compressed video quality analysis: On the example of no-reference metric niqe. *arXiv preprint arXiv:1907.03842*, 2019.